



Di-substituted pyridinyl aminohydantoin s as potent and highly selective human β -secretase (BACE1) inhibitors

Michael S. Malamas^{a,*}, Keith Barnes^b, Matthew Johnson^b, Yu Hui^b, Ping Zhou^a, Jim Turner^c, Yun Hu^c, Erik Wagner^c, Kristi Fan^a, Rajiv Chopra^d, Andrea Olland^d, Jonathan Bard^c, Menelas Pangalos^c, Peter Reinhart^c, Albert J. Robichaud^a

^a Department of Chemical Sciences, Wyeth Research, CN 8000, Princeton, NJ 08543-8000, USA

^b Albany Molecular Research, Albany, NY, USA

^c Neuroscience, Wyeth Research, CN 8000, Princeton, NJ 08543-8000, USA

^d Department of Chemical Sciences, Wyeth Research, 200 Cambridge Park Drive, Cambridge, MA 02140, USA

ARTICLE INFO

Article history:

Received 14 October 2009

Revised 30 November 2009

Accepted 2 December 2009

Available online 6 December 2009

Keywords:

Alzheimer's disease (AD)

BACE1 inhibitors

β -Amyloid peptide (A β)

Aminohydantoin s

ABSTRACT

The identification of highly selective small molecule di-substituted pyridinyl aminohydantoin s as β -secretase inhibitors is reported. The more potent and selective analogs demonstrate low nanomolar potency for the BACE1 enzyme as measured in a FRET assay, and exhibit comparable activity in a cell-based (ELISA) assay. In addition, these pyridine-aminohydantoin s are highly selectivity (>500 \times) against the other structurally related aspartyl proteases BACE2, cathepsin D, pepsin and renin.

Our design strategy followed a traditional SAR approach and was supported by molecular modeling studies based on the previously reported aminohydantoin **3a**. We have taken advantage of the amino acid difference between the BACE1 and BACE2 at the S2' pocket (BACE1 Pro₇₀ changed to BACE2 Lys₈₆) to build ligands with >500-fold selectivity against BACE2. The addition of large substituents on the targeted ligand at the vicinity of this aberration has generated a steric conflict between the ligand and these two proteins, thus impacting the ligand's affinity and selectivity. These ligands have also shown an exceptional selectivity against cathepsin D (>5000-fold) as well as the other aspartyl proteases mentioned. One of the more potent compounds (**S**)-**39** displayed an IC₅₀ value for BACE1 of 10 nM, and exhibited cellular activity with an EC₅₀ value of 130 nM in the ELISA assay.

© 2009 Elsevier Ltd. All rights reserved.

1. Introduction

Alzheimer's disease (AD) is a progressive, neurodegenerative disease of the brain and is recognized as the leading cause of dementia. At the early stage, AD is associated with gradual loss of cognition that leads to complete deterioration of cognitive, and behavioral functions and ultimately death. The pathological hallmarks of AD include the extracellular deposition of β -amyloid peptide (A β), which leads to aggregation and plaque formation, and the abnormal hyperphosphorylation of tau protein, which leads to the intracellular formation of neurofibrillary tangles.^{1,2} β -Amyloid deposits are predominately composed of the A β peptides (A β , 39–43 residues) resulting from the endoproteolysis of the amyloid precursor protein (APP).^{3,4} Neurofibrillary tangles are intracellular aggregates of the microtubule associated protein tau.⁵ A β peptides result from the sequential cleavage of APP, first at the N-terminus by β -secretase enzyme (β -site APP cleaving enzyme, BACE1),^{6,1} followed at the C-terminus by one or more γ -

secretase complexes (intramembrane aspartyl proteases),⁷ as part of the β -amyloidogenic pathway. During this process, two β -secretase cleavage products are produced; a secreted ectodomain fragment named APPsol, and the membrane bound C-terminal fragment C99 of APP. Following β -secretase cleavage, a second protease, γ -secretase, cleaves C99 to generate the toxic A β peptides (A β , 39–43 residues) which are secreted from the cell. Although, the cause of AD remains unknown, a large body of evidence is beginning to accumulate that highlights the central role of A β in the pathogenesis of the disease.^{8–11} Thus, processes that limit A β production and deposition by preventing formation, inhibiting aggregation, and/or enhancing clearance may offer effective treatments for AD. Since β -secretase mediated cleavage of APP is the first and rate-limiting step of the amyloidogenic possessing pathway, BACE1 inhibition is considered a prominent therapeutic target for treating AD by diminishing A β peptide formation in AD patients.

Recently, we have disclosed the discovery of small molecule aminohydantoin s as potent BACE1 inhibitors.¹² In early SAR investigations we quickly learned that the truncation of the tetrahydropyrimidine portion of the high-throughput screening hit **1** (Fig. 1)

* Corresponding author. Tel.: +1 732 2744428.

E-mail address: malamam@wyeth.com (M.S. Malamas).

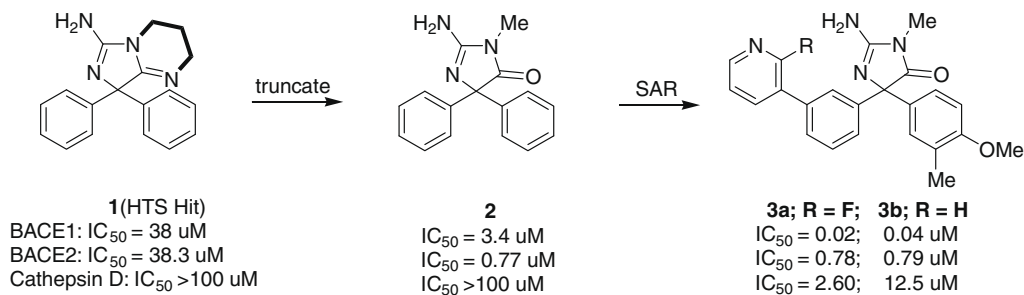


Figure 1.

which led to the more compact aminohydantoin **2**, possessed a 10-fold enhancement in potency (IC₅₀ = 3.4 μM). Soon afterward we carried out detailed structure–activity relationship studies¹³ around compound **2** that ultimately led to compound **3a**, which resulted in 1900-fold improvement of ligand affinity (**3a** vs **1**) for the BACE1 enzyme (IC₅₀ = 20 nM; Fig. 1). In addition, derivative **3a** has demonstrated about 40- and 100-fold selectivity against the close related aspartyl proteases BACE2 and cathepsin D, respectively. This modest selectivity over these two enzymes was a consequence of the initial SAR development, but not one that was focused on as a primary endpoint.

The physiological functions of BACE2 have yet to be fully characterized, and although BACE1/BACE2 double knockout mice have been reported to be viable¹⁴ selective inhibitors against BACE2 are highly desirable to avoid potential side effects in human clinical trials. More importantly, selectivity against cathepsin D was deemed to be essential to the clinical development of BACE1 inhibitors, since cathepsin D plays a critical role in cellular processes and functions as a positive mediator in apoptosis.¹⁵

In an effort to further enhance the selectivity of the aminohydantoin BACE1 inhibitors, we have closely examined the differences of the amino acid sequences of BACE1 and BACE2 as it regards binding of potential ligands to the active site. Not unexpectedly, the catalytic domain of BACE1 is similar to that of the BACE2 with 79% sequence identity within the active site. However, an overlay of the X-ray structure of BACE1 complexed with **1** and the homology model of BACE2 (Fig. 2) has revealed several amino acid differ-

ences between the two proteins at the extended ligand binding pocket. In particular, we have considered that the residue differences (BACE1 Pro₇₀ is replaced by BACE2 Lys₈₆) among the two proteins at the S2' pocket as a genuine opportunity for SAR investigation to potentially improve a ligand's selectivity. This continuing interest in this part of the extended BACE pocket is noteworthy as we have demonstrated in earlier SAR studies with aminohydantoin **3b** that interaction between the ligand and the enzyme at the S2' region might contribute to the ligand's selectivity.¹³

In this paper, we report our efforts to develop BACE1 inhibitors with enhanced selectivity against BACE2, by methodologically exploring the SAR around the S2' pocket of the enzyme. As described, our intent was to capitalize on the residue differences between the BACE1 and BACE2 enzymes in this micro-region and investigate the feasibility of rationally designing highly selective ligands.

2. Chemistry

The compounds needed to delineate the SAR for this study were prepared according to synthetic Scheme 1. In general, two routes were used for the formation of biaryl acetylenes **5**. In route a, Sonogashira coupling¹⁶ of disubstituted 4-ethynylpyridines **4** with 1-bromo-3-iodobenzene afforded acetylenes **5** in 75% yield. Alternatively, for enhanced SAR diversity, bromo-pyridines used in route b, where palladium-catalyzed cross coupling reaction of 1-bromo-3-iodobenzene with ethynyl(trimethyl)silane furnished adduct **6**, which upon hydrolysis to the corresponding phenyl-acetylene **7**, and further Sonogashira coupling with bromo-pyridines **8** afforded acetylenes **5** in 43% yield over the three steps. Oxidation of acetylenes **5** with potassium permanganate in the presence of magnesium sulfate and sodium bicarbonate furnished diketones **9**, in 75% yield. These 1,2 di-substituted diketones were converted to the aminohydantoins **10** upon treatment with 1-methylguanidine in the presence of potassium carbonate in excellent yields.¹³ Palladium-catalyzed cross coupling reaction of aminohydantoins **10** with any number of heteroaryl boronic acids **11** (Suzuki coupling¹⁷) in the presence of suitable Pd(0) or Pd(II) catalysts produced the desired products **12**.

The required key starting acetylenes, **4** and 4-bromopyridines **8** (Scheme 1) were either commercially available or prepared according to Scheme 2, employing Methods A–E. In Method A, 2-alkyl pyridines **14** were assembled according to the reaction conditions first reported by Comin's,¹⁸ where initial activation of the pyridines **13** with phenyl chloroformate followed by the addition of a Grignard reagent and oxidation with *o*-chloranil to furnish the desired adducts **14**, in 53% yield. Sonogashira coupling of pyridines **14** with ethynyl(trimethyl)silane and hydrolysis, as before, afforded acetylenes **15**. In Method B, 2,6-dimethylpyridin-4-ol was treated with phosphorus oxychloride to yield 4-chloropyridine **17**, which upon

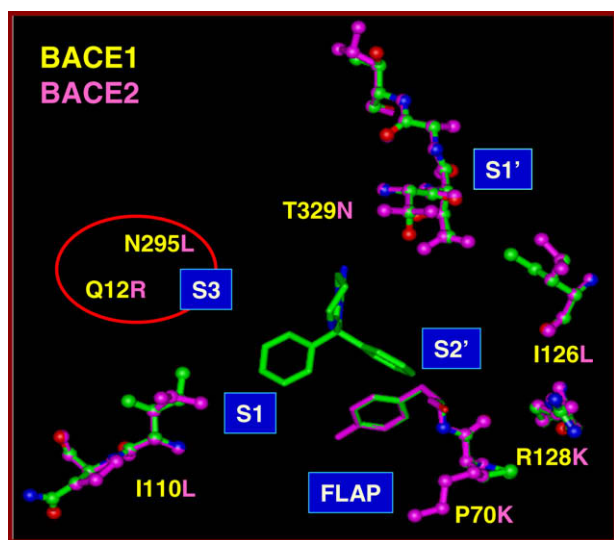
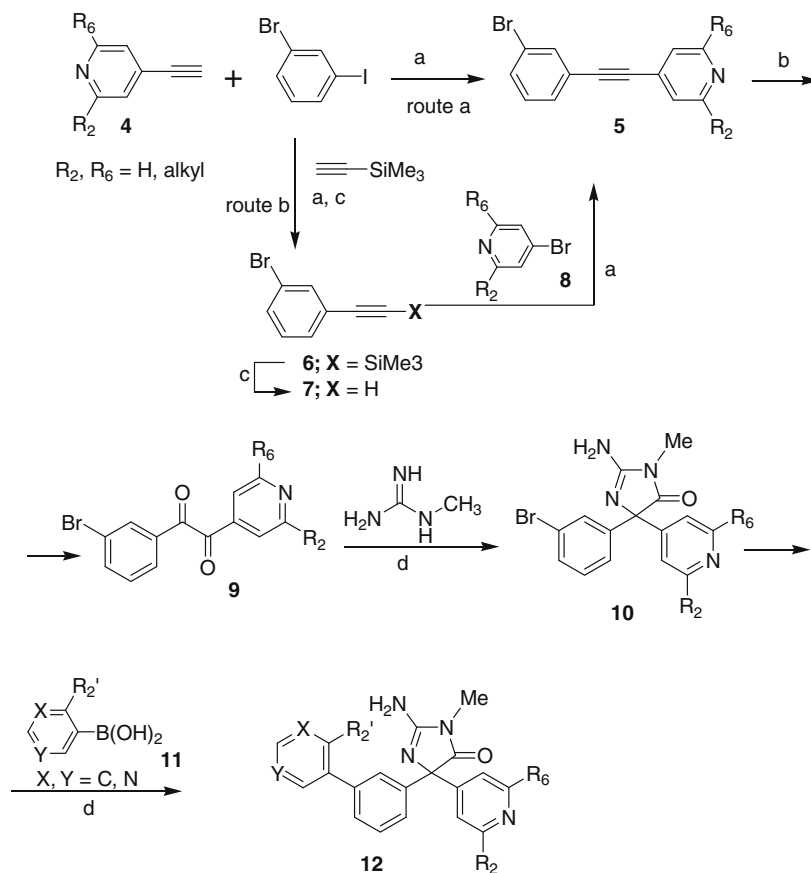


Figure 2. Crystal structure of BACE1 complexed with **1** (shown in green) and BACE2 homology (shown in magenta) are overlaid. Key amino acid differences between BACE1 (yellow) and BACE2 (magenta) are highlighted.



Scheme 1. Reagents and conditions: (a) Pd(PPh₃)₂Cl₂, CuI, Et₃N, DMF; (b) K₂CO₃, MeOH; (c) KMnO₄, NaHCO₃, MgSO₄, acetone; (d) methylguanidide-HCl, Na₂CO₃, EtOH, water; (e) aryl or heteroaryl boronic acids Pd(PPh₃)₄, Na₂CO₃, 1,2-diethoxyethane, water.

palladium-catalyzed coupling with 2-methylbut-3-yn-2-ol and subsequent hydrolysis with potassium hydroxide¹⁹ afforded acetylene **18**, in 25% yield over the three steps. In Method C, 4-bromo-2,6-dimethylpyridine **19** was alkylated with methyl iodide in the presence of lithium di-isopropyl amide²⁰ to furnish bromo-pyridine **20**, in 76% yield. In Method D, condensation of pentane-2,4-dione with methyl 2-methylpropanoate in the presence of sodium hydride, was followed by treatment with ammonium hydroxide to afford pyridin-4(1H)-one **22**²¹, in 53% yield over the two steps. Compound **22** was converted to **23** upon treatment with phosphorus oxybromide. In Method E, self-condensation of 3-oxopentane-dioic acid under acidic conditions furnished 2,6-diethyl-4H-pyran-4-one²² **25**, which was then treated with ammonium hydroxide²³ and phosphorous oxybromide to afford the desired product **27**, in 38% yield over the three steps.

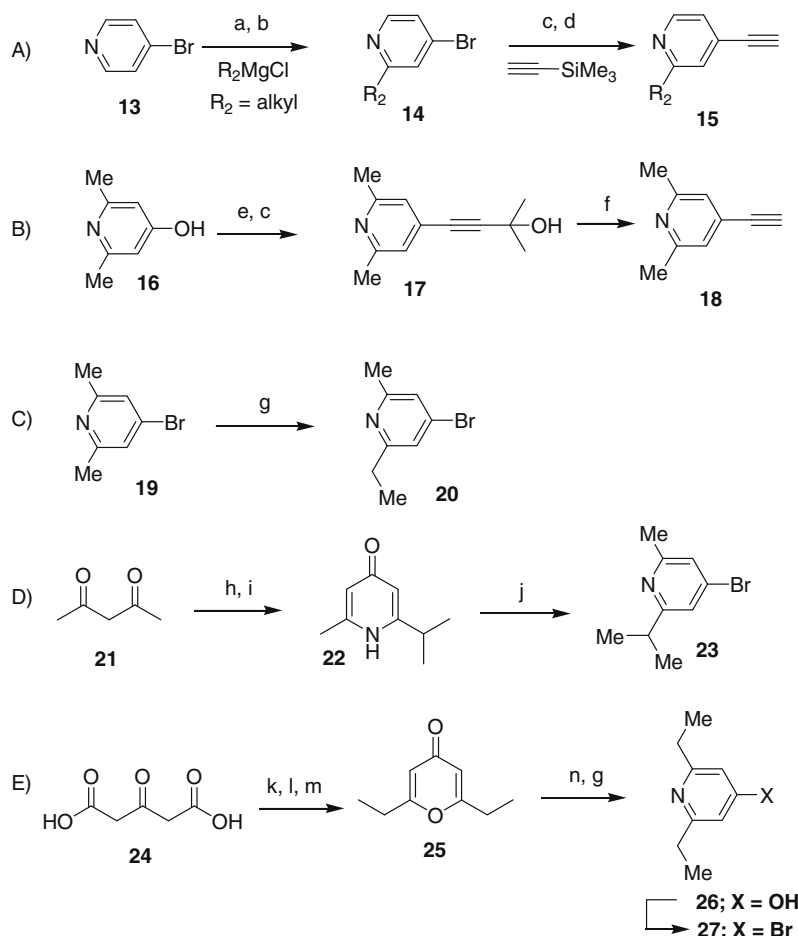
3. Results and discussion

With the necessary tools needed to fully investigate the SAR, the diverse array of compounds were profiled for their potency at the target enzyme, BACE1, as well as the closely related enzyme sites that were the focus of this investigation. The primary screening assays utilized for the program were homogenous, continuous fluorescence resonance energy transfer (FRET) protocols, representing competitive inhibition for BACE1, BACE2, cathepsin D, pepsin and renin.²⁴ The BACE1 and BACE2 activities were based on the cleavage of peptide substrate Abz-SEVNLDAEFR-Dpa (Swedish substrate), while peptide substrate MOCac-GKPILFFRLK (Dnp)-D-R-NH₂ was used for cathepsin D and pepsin, and peptide substrate

RE(EDANS)-IHPFHLVIHTK(DABCYL)-R for renin. Kinetic rates were calculated and IC₅₀ values were determined by fitting the % inhibition, as a function of compound concentration, to the Hill equation ($y = ((B * Kn) + (100 * xn)) / (Kn + xn)$). In practice, we have routinely screened all prepared compounds for BACE1, BACE2 and cathepsin D inhibition and then selected compounds were assayed in the pepsin and renin screens, based on their meeting the screening protocol for affinity to the target. These data are reported in Tables 1 and 2.

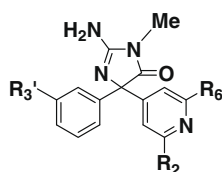
Cellular potency of advancing compounds was done via a cell-based A β inhibition (A β 40 or A β 42) in an enzyme-linked immune sandwich assay (ELISA) in Chinese Hamster Ovary (CHO) cells, recombinantly expressing human wild-type APP (CHO-wt). The concentration at which the cellular production of A β 40 or A β 42 was reduced by 50% (EC₅₀) was determined and reported in the data tables. Potential compound toxicity was assessed via mitochondrial function using a MTS readout (MTS kit from Promega) and values are represented as LD₅₀ or the dose of compound that resulted in 50% of control signal.

In this report, we have undertaken studies to methodically investigate the SAR of the aminohydantoin at the S2' pocket of the enzyme. As stated, our goal was to develop selective BACE1 inhibitors, by taking advantage of the amino acid difference between the BACE1 and BACE2 (BACE1 Pro₇₀ is replaced by BACE2 Lys₈₆) enzymes in this region. Towards this objective, we have used X-ray structures of BACE1 co-crystallized with various ligands and molecular modeling studies to help us in the design of such inhibitors. The initial unsubstituted baseline pyridine analog **28** showed a modest threefold improvement in selectivity for BACE1 vs phenyl derivative **2**. As we have described in great detail in our previous



Scheme 2. Methods A–E. Reagents and conditions: (a) R_2MgCl , $PhOCOCl$, THF; (b) *o*-chloranil, AcOH, toluene; (c) $Pd(PPh_3)_2Cl_2$, CuI, Et_3N , DMF; (d) K_2CO_3 , MeOH; (e) $POCl_3$; (f) KOH, toluene; (g) LDA, THF, MeI; (h) NaH, methyl 2-methylpropanoate, DME; (i) NaOH; (j) $POBr_3$; (k) H_2SO_4 ; (l) Na_2CO_3 , AcOH; (m) HCl; (n) NH_4OH .

Table 1
Pyridine-aminohydantoin



Compd	R_2	R_6	R_3'	BACE1 IC_{50}^a (μM)	BACE2 IC_{50} (μM)	Cathepsin D % inh. ^b at 100 μM	ELISA EC_{50}^a (μM)
28	H	H	H	2.68	2.01 ± 0.4	10	5.5 ± 0.9
29	H	H	Ph	0.13 ± 0.05	0.14 ± 0.04	$IC_{50} = 30 \pm 7.4 \mu M$	0.9 ± 0.4
30	H	H	3-Pyridine	0.06 ± 0.01	0.48 ± 0.15	45	0.3 ± 0.05
31	Me	H	3-Pyridine	0.1 ± 0.002	1.17	44	3.8 ± 1.3
32	Me	H	5-Pyrimidine	0.08 ± 0.001	2.2 ± 1.04	45	2.3 ± 1
33	Et	H	5-Pyrimidine	0.03 ± 0.01	1.02	49	0.9 ± 0.16
34	<i>i</i> -Pr	H	5-Pyrimidine	0.07 ± 0.01	6.13	47	1.9 ± 0.36
35	Me	Me	5-Pyrimidine	0.14 ± 0.01	24.1	14	3.7 ± 1.2
36	Et	Me	5-Pyrimidine	0.15 ± 0.03	28% at 12.5 μM	17	1.9 ± 0.3
37	<i>i</i> -Pr	Me	5-Pyrimidine	0.3 ± 0.14	24% at 25 μM	29	1.5 ± 0.14
38	Et	Et	5-Pyrimidine	0.04 ± 0.009	23.6	32	0.85 ± 0.5
S-38	Et	Et	5-Pyrimidine	0.03 ± 0.003	38% at 12.5 μM	22	0.27 ± 0.07
R-38	Et	Et	5-Pyrimidine	48% at 5 μM	11 ± 2.7	31	>2500
S-39	Et	Et	3-(2F-Pyridine)	0.01 ± 0.005	6.7 ± 0.8	$IC_{50} = 54 \pm 2 \mu M$	0.13 ± 0.04

^a IC_{50} and EC_{50} values are the means of at least two experiments \pm SD.

^b Experiments were performed in triplicate.

work,¹² molecular modeling and X-ray crystallographic studies have shown that building off the meta-position of the phenyl moi-

ety (occupying the S1 pocket) of potent biphenyl aminohydantoin derivatives would allow for projection directly towards the unoc-

Table 2
Pepsin and renin inhibition of selected compounds

Compd	Pepsin % inh. ^a at 200 μ M	Renin % inh. at 200 μ M
36	Inactive	Inactive
37	Inactive	Inactive
S- 38	9	Inactive
S- 39	13	26

^a Experiments were performed in triplicate.

cupied S3 region (see Fig. 3). This was proposed to have comparable effects in the pyridine series, and to that end, we have introduced a phenyl group at the meta-position of the phenyl moiety. Not surprisingly, that led to a 20-fold improvement in potency (**29** vs **28**), confirming this hypothesis. The analogous pyridine analog **30** was approximately 45-fold better for BACE1 (**30** vs **28**), again mirroring the previous SAR results. To confirm our modeling calculations and our hypothesis, **30** was co-crystallized with BACE1. As illustrated in Figure 4, the pyridine moiety projects deep into S3 pocket and makes a water-bridge contact with Ser229 through the buried water found near the catalytic site of the enzyme. This water-bridge interaction together with the additional van der Waals contacts between the ligand and the enzyme backbone at the S3 region are proposed to account for the ligand's increased potency. The X-ray structure also confirms, as before, that the amino group of the ligand interacts with both aspartic acids (Asp32 and Asp228) and the N3 nitrogen of the imidazole ring interacts with Asp32 via a hydrogen-bonding network. Furthermore, the BACE1:**30** structure indicates that the pyridine nucleus projecting into the S2' pocket makes a hydrogen-bonding contact with residue Trp76, and may be partly responsible for the increased potency. Compound **30** exhibited modest selectivity (~8-fold) against BACE2, and it was poorly active against cathepsin D (45% inhibition at 100 μ M). The importance of sustained activity in the cell was not lost during this investigation. Pyridine **30** tracked well with its increased molecular binding with EC₅₀ values of 300 nM in the cell-based ELISA assay.

Close examination of the BACE1:**30** X-ray structure revealed a key opportunity that we believed would allow for selectivity optimization between BACE1 and BACE2. We hypothesized that substitution at position 2 of the pyridine group located in the S2' pocket,

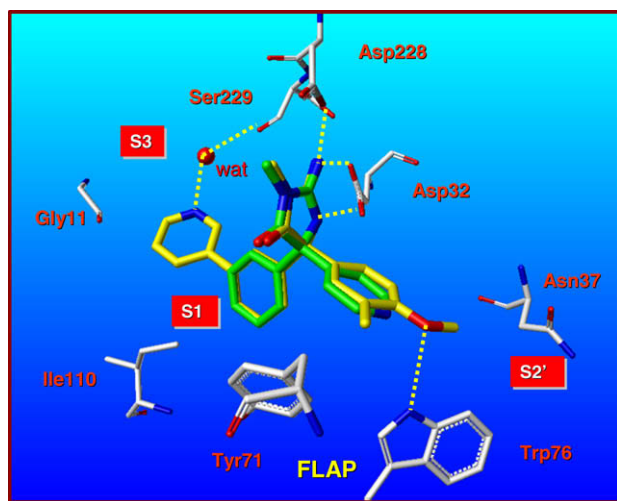


Figure 3. Crystal structure of BACE1 complexed with **3b**¹³ (shown in yellow) and pyridine **28** (shown in green) are overlaid. Key hydrogen-bonding interactions between ligand **3b** and protein at the catalytic aspartic acids Asp32 and Asp228, Trp76 at the S2' region, and the water-bridge to Ser229 are highlighted with yellow dashed lines.

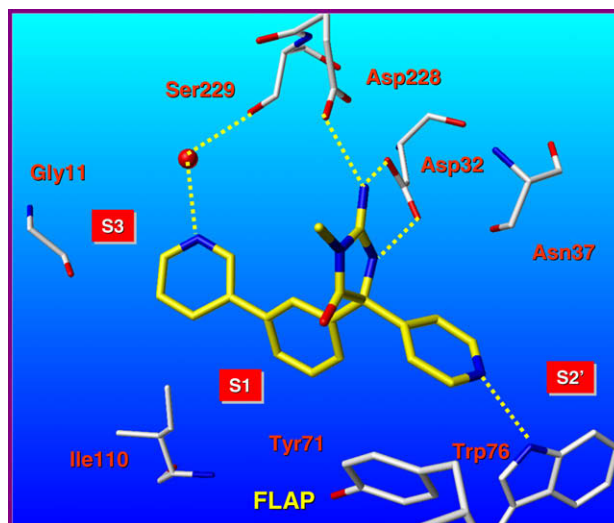


Figure 4. Crystal structure of BACE 1 complexed with **30**. Key hydrogen-bonding interactions between ligand **30** and protein at the catalytic aspartic acids Asp32 and Asp228, Trp76 at the S2' region, and the water-bridge to Ser229 are highlighted with yellow dashed lines.

offered an avenue to improve the BACE1 selectivity of **30** by targeting the BACE1 Pro₇₀ to BACE2 Lys₈₆ difference and generating a steric conflict between the ligand and the backbone of the BACE2 enzyme. To our satisfaction, introduction of a methyl group (entry **31**; Table 1) at position 2 of the pyridine nucleus modestly affected the ligand potency (two-fold decrease) for BACE1, while slightly improving the ligand's selectivity (about two-fold) against BACE2. Replacement of the pyridine nucleus projecting into the S3 with a pyrimidine moiety (**32**) resulted in an additional enhancement (two-fold) of the ligand's selectivity. With these initial results supporting our hypothesis, we further increased the size of the ortho-substituent of the pyridine moiety that projects into the S2' pocket. The derivative bearing an ethyl group at position 2 was approximately 34-fold selective against BACE2 (entry **33**), showing a marked improvement in selectivity, while the even bulkier isopropyl moiety (entry **34**) demonstrated broader selectivity (87-fold vs BACE2). The cathepsin D selectivity of these analogs tracked very well with the previous findings, with all compounds exhibiting weak affinity (IC₅₀ ~100 μ M) for this site.

One cannot neglect the possibility that mere rotation of the pyridine ring in this S2' pocket would move the alkyl group offering the apparent selectivity from interacting with the backbone of the BACE2 enzyme. This would effectively diminish the utility of the 2-substituted pyridyl adducts, that being to cause an unfavorable interaction with the BACE2 backbone. Furthermore, molecular modeling studies have indicated that this binding mode (rotation of the alkyl group away from the Lys86 in BACE2) would be accommodated by the enzyme sites of both BACE1 and BACE2. In order to maintain a sterically biased effect in this pocket, we have endeavored to prepare di-substituted analogs at positions 2 and 6 of the pyridine nucleus to abrogate the enzymes ability to remove the offending interaction. To that end, introduction of methyl groups at positions 2 and 6 of the pyridine nucleus was executed and this derivative produced a marked increase in ligand selectivity (170-fold; **35** vs **31**). Having confirmed our hypothesis that the 2,6-pyridine substitutions are optimal to effectively target the Pro₇₀ to Lys₈₆ difference and improve BACE1 selectivity, we have systematically varied the size and steric encumbrance of the substituents at the 2,6-positions of the pyridine nucleus to further optimize the ligand's selectivity. This can be seen with both di-substituted analogs, ethyl-methyl (**36**) and isopropyl-methyl (**37**), as they

possess only marginal affinity ($\sim 28\%$ at $25 \mu\text{M}$) for BACE2, while the BACE1 affinity was practically unaffected. The bulkier isopropyl group has produced a slight ~ 2 -fold reduction of the BACE1 affinity (**36** vs **37**). Furthermore, the ethyl–ethyl di-substituted analog **38** was the most selective ligand, showing 590-fold preference for BACE1. Next, we have replaced the pyrimidine nucleus of **38** with the previously optimized 2-F-pyridyl moiety,¹⁴ which was discovered during the optimization of the SAR studies of compound **3a**. The 2,6-diethyl pyridyl analog **39** showed high potency for BACE1 ($\text{IC}_{50} = 10 \text{ nM}$) and exquisite selectivity ($670\times$) against BACE2. Compound **39** was also highly selective $>5000\times$ against cathepsin D. Furthermore, the cell-based activity of pyridine **39** tracked well compared to its molecular binding with an EC_{50} value of 130 nM in the ELISA assay.

In support of our modeling studies and design of selective BACE1 ligands, compound (*S*)-**38** was co-crystallized with the BACE1 enzyme. Overlapping of the X-ray crystal structures of compounds (*S*)-**38** and **30** bound to the enzyme indicated a nearly perfect superimposition of these two ligands (Fig. 5). Close examination of these overlapping structures, however, has revealed a shift of the ‘flap’ loop region of the protein backbone of the enzyme resulting in a more open orientation of the loop (approximately 5 \AA shift vs apo-position) for the more selective compound (*S*)-**38**. Notice that with the unsubstituted ligand **30**, the loop is in a more closed orientation (apo-position), which has obvious profound impact on the selectivity versus BACE2. The open orientation of the ‘flap’ region in the BACE1:(*S*)-**38** structure is perhaps attributed to the steric influence exerted by the 2-ethyl group of the $\text{S}2'$ -pyridine moiety. As discussed previously, the protein amino acid sequences of the ‘flap’ loops of the BACE1 and BACE2 proteins differ in the $\text{S}2'$ pocket (BACE1 Pro₇₀ is replaced by BACE2 Lys₈₆ and BACE1 Arg₁₂₈ is replaced by Lys in BACE2) at close proximity to the bound ligand. This minor amino acid difference together with the dynamic motion of the ‘flap’ loop upon ligand engagement apparently influences the ligand/protein contacts and impedes the ligand’s affinity for the BACE2 site, thus resulting in increased selectivity. Additionally, both ethyl groups make favorable contact with other residues of the $\text{S}2'$ pocket backbone of the BACE1 enzyme, thus contributing to the ligand’s affinity. More specifically, the crystal structure shows that the ethyl group

that projects towards the FLAP region interacts with Val69, while the distal ethyl moiety interacts with Ser35. Furthermore, The BACE1:(*S*)-**38** structure revealed, similar to the previous X-ray findings,¹² that the aminohydantoin portion of the ligand directly interacts with both catalytic-site aspartic acids (Asp32 and Asp228) via a hydrogen-bonding network, and the pyrimidine moiety of the ligand extends deep into the $\text{S}3$ pocket and makes a water-bridge contact with Ser229. Lastly, the nitrogen of the pyridine nucleus located at the $\text{S}2'$ pocket makes a hydrogen-bond interaction with residue Trp76.

Furthermore, an investigation of the chiral preference of the racemic mixtures of this class of compounds, once separated, showed a clear preference for the *S*-enantiomer [see (*S*)-**38** vs (*R*)-**38**]. This was apparent as the crystal structures and modeling studies bore this out. For the less active enantiomer, one could envision keeping the respective $\text{P}1$ – $\text{P}3$ and $\text{P}2'$ side-chains in their designed pockets, but in so doing, the aminohydantoin would be flipped into an unfavorable confirmation and pressed into the backbone of the active site of the enzyme.

To confirm the more general specificity of these ligands for the BACE1 enzyme, a representative set of compounds were evaluated for inhibition of renin and pepsin aspartyl proteases. As shown in Table 2, all compounds demonstrated weak inhibition for these closely related targets confirming their potential as selective BACE1 ligands.

4. Conclusions

In this report, we have described a detailed and stepwise exploration of substituted pyridine-aminohydantoin that led to the discovery of highly potent and selective BACE1 inhibitors. The more potent selective analogs demonstrate low nanomolar potency ($\text{IC}_{50} = 10 \text{ nM}$) for BACE1 in a FRET assay, and exhibit comparable activity in a cell-based (ELISA) assay. In addition, these aminohydantoin show >500 -fold selectivity toward the other structurally related aspartyl proteases BACE2, cathepsin D, pepsin, and renin.

Our design strategy followed a traditional SAR approach and was supported by molecular modeling studies based on the previously reported aminohydantoin **3**. We have taken advantage of the amino acid difference between the BACE1 and BACE2 enzymes at the $\text{S}2'$ pocket (BACE1 Pro₇₀ changed to BACE2 Lys₈₆) to build ligands with >500 -fold selectivity against BACE2. The addition of large steric substituents at the vicinity of this mutation has generated an apparent conflict between the ligand and the BACE2 enzyme backbone, thus affecting the ligand’s affinity and selectivity. These ligands have also shown a distinguished selectivity against cathepsin D (>5000). One of the more potent compounds (*S*)-**39** displayed an IC_{50} value for BACE1 of 10 nM , and exhibited cellular activity with an EC_{50} value of 130 nM in the ELISA assay. Ligand (*S*)-**39** also showed >500 -fold selectivity the other related aspartyl proteases BACE2, cathepsin D, pepsin, and renin.

5. Experimental section

5.1. Chemistry

Melting points were determined in open capillary tubes on a Mel-Temp-II apparatus, and reported uncorrected. ¹H NMR spectra were determined in the cited solvent on a Varian Unity or Varian Inova (400 MHz) instrument, with tetramethylsilane as an internal standard. Chemical shifts are given in ppm and coupling constants are in hertz. Splitting patterns are designated as follows: s, singlet; br s, broad singlet; d, doublet; t, triplet; q, quartet; m, multiplet. The infrared spectra were recorded on a AVATAR 360 Nicolet spectrophotometer as KBr pellets or as solutions in chloroform. Mass

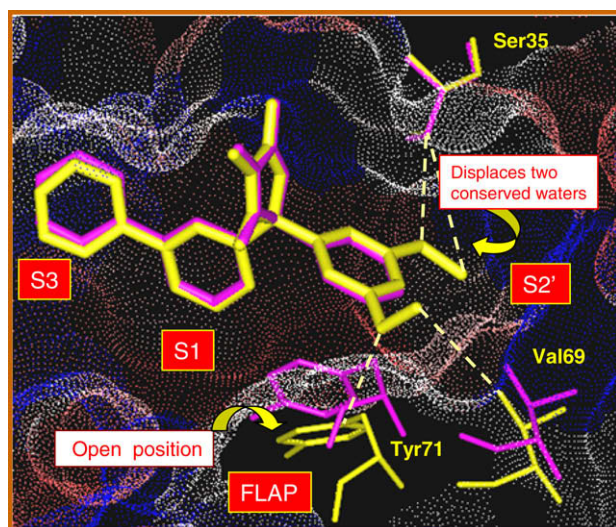


Figure 5. Crystal structures of BACE 1 complexed with (*S*)-**38** (shown in yellow) and **30** (shown in magenta) are overlaid. Movement of Tyr71 from the closed position in complex **30** to the open orientation in complex with (*S*)-**38** is shown. Key hydrogen-bonding interactions between the ligand and residues Tyr71, Val69 and Ser35 at the $\text{S}2'$ region are shown in yellow dotted lines.

spectra were recorded on a Micromass LCT, Waters spectrometer. Elemental analyses (C, H, N) were performed on a Perkin–Elmer 240 analyzer and all compounds are within $\pm 0.4\%$ of theory unless otherwise indicated. HPLC techniques and high resolution mass spectrometry were used to determine the purity of compounds outside the range of the elemental analysis assessment. Purity of all final products was $>96\%$ as determined by HPLC and/or combustion analysis. Purity was determined by HPLC analysis using the following protocols. Method A: Mobile Phase A: 10 mM ammonium formate in water (pH 3.5); B: 50:50 ACN/MeOH; solvent gradient 85:15 to 5:95 A:B in 2 min., hold 1.25 min, re-equilibrate 0.5 min; flow rate 1.1 mL/min; Column Agilent SB C18 1.8 μM , 3.0×50 mm; temperature 45 °C; detection at 210–370 nm. Method B: mobile phase water with A = 0.05% v/v trifluoroacetic acid, B = acetonitrile with 0.05% v/v trifluoroacetic acid; solvent gradient 90:10 to 10:90 A:B in 20 min; flow rate 1.0 mL/min; Waters Symmetry C18 column (4.6×250 mm) with UV detection at 254 nm. All products, unless otherwise noted, were purified by ‘flash chromatography’ with use of 220–400 mesh silica gel. Thin-layer chromatography was done on Silica Gel 60 F-254 (0.25 mm thickness) plates. Visualization was accomplished with UV light and/or 10% phosphomolybdic acid in ethanol. The hydration was determined by the Karl Fischer titration, using a Mitsubishi moisture meter Model CA-05. Unless otherwise noted, all materials were obtained commercially and used without further purification. All reactions were carried out under an atmosphere of dried argon or nitrogen.

5.2. Representative synthetic protocols of the aminohydantoins shown in Scheme 1 are described below

5.2.1. Preparation of 4-[(3-bromophenyl)ethynyl]pyridine (5, $R_2, R_6 = \text{H}$, route a)

To a solution of 1-bromo-3-iodobenzene (5.0 g, 17.6 mmol) in DMF (50 mL) were added dichlorobis(triphenylphosphine)palladium (0.23 g, 0.29 mmol), copper iodide (0.03 g, 0.16 mmol), triethylamine (6.7 mL, 48.5 mmol) and 4-ethynylpyridine (1.0 mL, 9.7 mmol). The reaction mixture was heated at 65 °C for 3 h, and then cooled and quenched with water (100 mL). The aqueous mixture was extracted with EtOAc (3×50 mL) and the combined organic extracts were washed with brine (50 mL), and dried over MgSO_4 . Evaporation of the solvents and purification by flash chromatography (silica gel, EtOAc/hexane 1:3) afforded 4-[(3-bromophenyl)ethynyl]pyridine as a yellow solid (1.9 g, 76% yield): $^1\text{H NMR}$ (300 MHz, $\text{DMSO}-d_6$) δ 7.38–7.40 (m, 1H, Ar-H), 7.49–7.51 (m, 2H, Ar-H), 7.6–7.61 (m, 1H, Ar-H), 7.65–7.65 (m, 1H, Ar-H), 7.81 (t, 1H, $J = 1.58$ Hz, Ar-H), 8.61–8.62 (m, 2H, Ar-H); MS m/z 258 ($\text{M}+\text{H}^+$); Anal. Calcd for $\text{C}_{13}\text{H}_8\text{BrN}$ $\times 0.1 \text{ H}_2\text{O}$: C, 60.07; H, 3.18; N, 5.38. Found: C, 60.02; H, 3.18; N, 5.1.

5.2.2. Preparation of 1-(3-bromophenyl)-2-pyridin-4-ylethane-1,2-dione (9, $R_2, R_6 = \text{H}$)

A solution of 4-[(3-bromophenyl)ethynyl]pyridine (1.81 g, 7.0 mmol) in acetone (63 mL) was added into a warm (40 °C) mixture of NaHCO_3 (0.35 g, 4.20 mmol) and MgSO_4 (1.26 g, 10.50 mmol) in water (63 mL). Potassium permanganate (2.43 g, 15.40 mmol) was added in one portion and the reaction mixture was stirred at room temperature for 4 min, poured into water (300 mL) and extracted with 1:1 Et_2O /hexane. The organic extracts were dried over MgSO_4 . Evaporation of the solvents afforded 1-(3-bromophenyl)-2-pyridin-4-ylethane-1,2-dione as a yellow solid (1.52 g, 75% yield): mp 88–90 °C; $^1\text{H NMR}$ (300 MHz, $\text{DMSO}-d_6$) δ 7.56–7.57 (m, 1H, Ar-H), 7.81–7.82 (m, 2H, Ar-H), 7.95–7.97 (m, 2H, Ar-H), 8.1 (t, 1H, $J = 1.71$ Hz, Ar-H), 8.86 (dd, 2H, $J = 4.39, 1.59$ Hz, Ar-H); MS m/z 289 ($\text{M}+\text{H}^+$). Anal. Calc for $\text{C}_{13}\text{H}_8\text{BrNO}_2$: C, 53.82; H, 2.78; N, 4.83. Found: C, 53.49; H, 2.73; N, 4.63.

5.2.3. Preparation of 2-amino-5-(3-bromophenyl)-3-methyl-5-(pyridin-4-yl)-3,5-dihydro-4H-imidazol-4-one (10, $R_2, R_6 = \text{H}$)

A suspension of 1-phenyl-2-pyridin-4-ylethane-1,2-dione (0.81 g, 3.8 mmol), *N*-methylguanidine hydrochloride (1.16 g, 4 mmol) and Na_2CO_3 (1.9 g, 18 mmol) in EtOH (80 mL), dioxane (62 mL) and water (18 mL) was stirred at 85 °C for 1 h. The reaction mixture was cooled to room temperature, poured into water and extracted with CHCl_3 (3×60 mL). The combined organic extracts were dried over MgSO_4 . Evaporation of the solvents and purification by flash chromatography (silica gel, dichloromethane/MeOH, 10:1) afforded 2-amino-5-(3-bromophenyl)-3-methyl-5-(pyridin-4-yl)-3,5-dihydro-4H-imidazol-4-one as an off-white solid (0.73 g, 53%): $^1\text{H NMR}$ (300 MHz, $\text{DMSO}-d_6$) δ 2.95 (s, 3H, Me), 6.83 (br s, 2H, NH_2), 7.34–7.3–7.35 (m, 1H, Ar-H), 7.36–7.38 (m, 2H, Ar-H), 7.43–7.45 (m, 2H, Ar-H), 7.6 (t, 1H, $J = 1.83$ Hz, Ar-H), 8.48 (dd, 2H, $J = 4.53, 1.71$ Hz, Ar-H); MS m/z 345 ($\text{M}+\text{H}^+$). Anal. Calcd for $\text{C}_{15}\text{H}_{13}\text{BrN}_4\text{O}$: C, 52.19; H, 3.58; N, 16.23. Found: C, 52.15; H, 3.79; N, 16.35.

5.2.4. Preparation of 2-amino-5-(2,6-diethylpyridin-4-yl)-3-methyl-5-[3-(pyrimidin-5-yl)phenyl]-3,5-dihydro-4H-imidazol-4-one (12, $R_2, R_6 = \text{Et}$, $R'_2 = \text{H}$, $\text{X}, \text{Y} = \text{N}$).

A mixture of 2-amino-5-(3-bromophenyl)-5-(2,6-diethylpyridin-4-yl)-3-methyl-3,5-dihydro-4H-imidazol-4-one (0.12 g, 0.297 mmol), pyrimidine-5-boronic acid (0.044 g, 0.355 mmol), tetrakis(triphenylphosphino)palladium(0) (0.018 g, 0.016 mmol) and sodium carbonate (0.083 g, 0.783 mmol) in ethylene glycol dimethyl ether (8 mL) and water (4 mL) was heated at reflux for 1 h. The mixture was cooled to room temperature, concentrated, and the residue partitioned between CH_2Cl_2 (50 mL) and water (50 mL). The layers were separated, and the aqueous layer was extracted with methylene chloride (2×25 mL) and the combined organic extracts were dried over Na_2SO_4 . Evaporation of the solvents and purification by flash chromatography (silica gel, 96:4:0.5 methylene chloride/methanol/concentrated ammonium hydroxide) afforded 2-amino-5-(2,6-diethylpyridin-4-yl)-3-methyl-5-(3-pyrimidin-5-ylphenyl)-3,5-dihydro-4H-imidazol-4-one as an off-white solid (0.059 g, 49% yield): mp 204.5 °C; $^1\text{H NMR}$ (300 MHz, CDCl_3) δ 1.26 (t, $J = 7.6$ Hz, 6H, $2 \times \text{CH}_2\text{CH}_3$), 2.76 (q, $J = 7.6$ Hz, 4H, $2 \times \text{CH}_2\text{CH}_3$), 3.14 (s, 3H, Me), 4.75 (br s, 2H, NH_2), 7.15 (s, 2H, Ar-H), 7.49 (m, 2H, Ar-H), 7.62 (s, 1H, Ar-H), 7.74 (s, 1H, Ar-H), 8.92 (s, 2H, Ar-H), 9.20 (s, 1H, Ar-H); MS m/z 401 ($\text{M}+\text{H}^+$). Anal. Calcd for $\text{C}_{23}\text{H}_{24}\text{NO}_6 \times 1\text{H}_2\text{O}$: C, 66.01; H, 6.26; N, 20.0. Found: C, 66.09; H, 6.20; N, 19.66.

5.2.5. Preparation of [(3-bromophenyl)ethynyl](trimethyl)silane (6, $\text{X} = \text{SiMe}_3$)

To a solution of 1-bromo-3-iodobenzene (4.1 g, 14.5 mmol) in DMF (50 mL) were added dichlorobis(triphenylphosphine)palladium (0.31 g, 0.43 mmol), copper iodide (0.055 g, 0.16 mmol), triethylamine (10 mL, 72.5 mmol) and ethynyl(trimethyl)silane (2.05 mL, 14.5 mmol). The reaction mixture was heated at 65 °C for 3 h, cooled at room temperature, and quenched with water (100 mL). The aqueous mixture was extracted with EtOAc (3×50 mL) and the combined organic extracts were washed with brine (50 mL), and dried over MgSO_4 . Evaporation of the solvents and purification by flash chromatography (silica gel, hexane) afford [(3-bromophenyl)ethynyl](trimethyl)silane as a yellow oil (3.0 g, 82% yield): $^1\text{H NMR}$ (300 MHz, $\text{DMSO}-d_6$) δ 0.19 (s, 3H, SiMe_3), 7.28–7.3 (m, 1H, Ar-H), 7.4(7.2-(m, 1H, Ar-H), 7.55–7.6 (m, 2H, Ar-H); MS m/z 252 ($\text{M}+\text{H}^+$).

5.2.6. Preparation of 1-bromo-3-ethynylbenzene (7, $\text{X} = \text{H}$)

To a solution of [(3-bromophenyl)ethynyl](trimethyl)silane (10 g, 39.5 mmol) in dichloromethane (150 mL) and ethanol (150 mL) was added Cs_2CO_3 (13 g, 39.9 mmol) at room temperature. After stirring for 4 h, the reaction mixture was diluted with

Et₂O (300 mL) and washed with water and brine. Evaporation of the solvents and distillation (2 psi, 55 °C) afforded a clear oil (6.8 g, 93.9% yield): ¹H NMR (300 MHz, DMSO-*d*₆) δ 4.29 (s, 1H, acetylene-H), 7.28–7.30 (m, 1H, Ar-H), 7.43–7.46 (m, 1H, Ar-H), 7.57–7.59 (m, 1H, Ar-H), 7.63–7.64 (m, 1H, Ar-H); MS *m/z* 180 M⁺. Anal. Calcd for C₈H₅Br: C, 53.08%; H, 2.78%; Found: C, 52.78%; H, 2.65.

5.2.7. Preparation of 4-[(3-bromophenyl)ethynyl]pyridine (5, R₂, R₆ = H, route b)

To a solution of 1-bromo-3-ethynylbenzene (0.8 g, 4.4 mmol) in DMF (20 mL) were added dichlorobis(triphenylphosphine)palladium (0.09 g, 0.13 mmol), copper iodide (0.09 g, 0.46 mmol), triethylamine (3.1 mL, 22 mmol) and 4-bromopyridine (1.05 g, 94.4 mmol). The reaction mixture was heated at 65 °C for 4 h, then cooled to room temperature and quenched with water (100 mL). The aqueous mixture was extracted with EtOAc (3 × 50 mL) and the combined organic extracts were washed with brine (50 mL), and dried over MgSO₄. Evaporation and purification by flash chromatography (silica gel, EtOAc/hexane 1:4) afforded 4-[(3-bromophenyl)ethynyl]pyridine as a yellow solid (0.6 g, 53%): ¹H NMR (300 MHz, DMSO-*d*₆) δ 7.38–7.40 (m, 1H, Ar-H), 7.49–7.51 (m, 2H, Ar-H), 7.6–7.61 (m, 1H, Ar-H), 7.65–7.65 (m, 1H, Ar-H), 7.81 (t, 1H, *J* = 1.58 Hz, Ar-H), 8.61–8.62 (m, 2H, Ar-H); MS *m/z* 258 (M+H)⁺. Anal. Calcd for C₁₃H₈BrN × 0.1 H₂O: C, 60.07%; H, 3.18%; N, 5.38%. Found: C, 59.92%; H, 3.12%; N, 5.23.

5.3. The preparation of the substituted pyridines shown in Scheme 2 were prepared according to the synthetic Methods A–E

5.3.1. Method A

5.3.1.1. Steps a and b. Preparation of 4-bromo-2-methylpyridine (14, R₂ = Me). To a cooled (–78 °C) suspension of 4-bromopyridine hydrochloride (5.0 g, 25.7 mmol) in anhydrous THF (90 mL) was added dropwise a solution of MeMgCl (3.0 M in THF, 21 mL, 63.0 mmol). After the addition, the reaction mixture was stirred at –78 °C for 15 min. Phenyl chloroformate (3.8 mL, 30 mmol) in THF (10 mL) was added slowly and the mixture was allowed to warm to room temperature. Afterwards, the reaction was cooled at 0 °C, quenched with saturated NH₄Cl and extracted with Et₂O. The combined organic extracts were successively washed with water, HCl (1 N), and brine. The organic extracts were dried over MgSO₄ and the solvents were evaporated. The residue was dissolved in anhydrous toluene (100 mL) and a solution of *o*-chloranil (7.8 g, 32 mmol) in AcOH (60 mL) was added dropwise and the mixture was stirred for 22 h. A red suspension was formed and it was then the mixture was made basic by using 10% NaOH until a black emulsion was obtained. The mixture was filtered through a Celite pad and washed with water. The organic layer was extracted three times with HCl (1 N). The combined aqueous extracts were basified with 50% NaOH and extracted with CH₂Cl₂. The combined organic extracts were dried over MgSO₄ and the solvents were removed under vacuum to afford 4-bromo-2-methylpyridine as yellow oil (2.35 g, 53% yield): ¹H NMR (300 MHz, DMSO-*d*₆) δ 2.4 (s, 3H, Me), 7.42 (1H, dd, *J* = 5.37, 1.95 Hz, Ar-H), 7.52 (d, 1H, *J* = 1.46 Hz, Ar-H), 8.3 (d, 1H, *J* = 5.37, Ar-H); MS *m/z* 171 M⁺.

5.3.1.2. Steps c and d. The preparation of 4-ethynyl-2-methylpyridine **15** (R₂ = Me; Scheme 2) was prepared from 4-bromo-2-methylpyridine (**14**, R₁ = Me) and ethynyl(trimethyl)silane according to the synthetic protocols described in Scheme 1.

5.3.2. Method B

5.3.2.1. Steps e and c. Preparation of 4-(2,6-dimethylpyridin-4-yl)-2-methylbut-3-yn-2-ol (17). 2,6-Dimethyl-4-hydroxypyridine (1.74 g, 14.1 mmol) was treated with phosphorous oxychloride (2.63 g, 0.17 mol) under N₂. The mixture was warmed to reflux for 1 h then cooled to room temperature. Excess phosphorous oxychloride was removed under reduced pressure, and the residue diluted with dichloroethane (50 mL). The mixture was again concentrated to provide 4-chloro-2,6-dimethylpyridine (2.0 g) as a red oil. This material was dissolved in DMF (65 mL) under N₂, and treated with bis(triphenylphosphino)palladium(II) chloride (315 mg, 0.45 mmol), triphenylphosphine (243 mg, 0.93 mmol), copper(I) iodide (268 mg, 1.42 mmol), triethylamine (11.1 g, 110 mmol), and 2-methyl-3-butyn-2-ol (2.43 g, 289 mmol). The mixture was heated at 100 °C overnight and cooled to room temperature. Ethyl acetate (400 mL) and water (200 mL) were added, the layers were separated, and the aqueous layer was extracted with ethyl acetate (2 × 100 mL). The combined organic layers were washed with 2% aq lithium chloride (2 × 150 mL), and dried Na₂SO₄. Evaporation of the solvents and purification by flash chromatography (silica gel, 100:0–98:2 methylene chloride/methanol) afforded 4-(2,6-dimethylpyridin-4-yl)-2-methylbut-3-yn-2-ol as a brown solid (0.96 g, 36% yield): ¹H NMR (300 MHz, CDCl₃) δ 1.61 (s, 6H, 2 × Me), 2.14 (s, 1H, Me), 2.50 (s, 6H, 2 × Me), 6.97 (s, 2H, Ar-H); MS *m/z* 190 (M+H)⁺.

5.3.2.2. Step f. Preparation of 4-ethynyl-2,6-dimethylpyridine (18). A solution of 4-(2,6-dimethylpyridin-4-yl)-2-methylbut-3-yn-2-ol (102 mg, 0.54 mmol) in toluene (5 mL) under N₂ was treated with powdered potassium hydroxide (51.0 mg, 0.91 mmol), and the mixture was heated at reflux for 1 h. The mixture was cooled to room temperature, diluted with ethyl acetate (100 mL) and water (100 mL), and the layers were separated. The aqueous layer was extracted with ethyl acetate (2 × 50 mL), and the combined organic extracts were dried over Na₂SO₄, filtered, and concentrated to afford 4-ethynyl-2,6-dimethylpyridine as a light orange solid (0.05 g, 70% yield): ¹H NMR (300 MHz, CDCl₃) δ 2.51 (s, 6H, 2 × Me); 3.20 (s, 1H, acetylene-H), 7.04 (s, 2H, Ar-H); MS *m/z* 132 (M+H)⁺.

5.3.3. Method C

5.3.3.1. Preparation of 4-bromo-2-ethyl-6-methylpyridine (20). To a solution of diisopropylamine (1.49 g, 14.8 mmol) in tetrahydrofuran (55 mL) at –78 °C was added dropwise *n*-butyllithium (10.2 mL of a 1.6 M solution in hexanes, 16.3 mmol). The mixture was stirred for 15 min at –78 °C, warmed to 0 °C for 15 min and then cooled to –78 °C. The solution of lithium diisopropylamide was then transferred via a cannula to a stirred solution of commercially available 4-bromo-2,6-dimethyl pyridine (2.75 g, 14.8 mmol) in tetrahydrofuran (30 mL) at –78 °C and the mixture stirred for 1 h. Methyl iodide (2.31 g, 16.3 mmol) was added and the reaction stirred for an additional 30 min. Saturated aqueous NH₄Cl (20 mL) was then added, and the mixture was allowed to warm to room temperature and then diluted with CH₂Cl₂ (200 mL) and water (100 mL). The organic layer was separated and washed successively with water (100 mL) and brine (100 mL), and dried over sodium sulfate. Evaporation of the solvents and purification by flash chromatography (silica gel, 90:10 hexanes/ethyl acetate) afforded 4-bromo-2-ethyl-6-methylpyridine as a yellow oil (2.26 g, 76% yield): ¹H NMR (300 MHz, CDCl₃) δ 1.28 (t, *J* = 7.6 Hz, 3H, CH₂CH₃), 2.50 (s, 3H, Me), 2.75 (q, *J* = 7.6 Hz, 2H, CH₂CH₃), 7.16 (s, 2H, Ar-H); MS *m/z* 200 (M+H)⁺.

5.3.4. Method D

5.3.4.1. Steps h and i. Preparation of 2-methyl-6-(propan-2-yl)pyridin-4(1H)-one (22). To a suspension of sodium hydride (2.00 g of a 60% dispersion in oil, 50.0 mmol) and ethylene glycol dimethyl ether (35 mL) at reflux was added dropwise a solution of acetyl acetone (1.00 g, 10.0 mmol) and methyl isobutyrate (1.53 g, 14.9 mmol) in ethylene glycol dimethyl ether (35 mL), at

a rate as to maintain gentle hydrogen evolution at a controllable rate. The reaction was then refluxed for a further 4 h and cooled to room temperature. The condenser was removed and replaced with a distillation head, vacuum was applied and the solvent (ca. 40 mL) was removed. The resulting slurry was diluted with diethyl ether (50 mL), cooled to 0 °C and quenched with water (50 mL). After separating the layers, the organic layer was washed with water (30 mL) and 1% NaOH (30 mL). Ice chips were added to the combined aqueous layer, followed by concentrated hydrochloric acid (10 mL). The mixture was extracted with ether (3 × 50 mL), and the combined organic extracts were dried Na₂SO₄. The resulting product 7-methyloctane-2,4,6-trione was then dissolved in concentrated NH₄OH (45 mL) and heated at reflux for 3 h. The reaction mixture was cooled and the solvents evaporated to afford 2-methyl-6-(propan-2-yl)pyridin-4(1H)-one as a red viscous oil (0.80 g, 53% yield): ¹H NMR (300 MHz, CDCl₃) δ 1.27 (d, *J* = 6.9 Hz, 6H, CHMe₂), 2.32 (s, 3H, Me), 2.84 (septet, *J* = 6.9 Hz, 1H, CHMe₂), 6.21 (s, 1H, olefinic-H), 6.17 (s, 1H, olefinic-H); MS *m/z* 152 (M+H)⁺.

5.3.4.2. Step j. Preparation of 4-bromo-2-methyl-6-(propan-2-yl)pyridine (23). A mixture of 2-methyl-6-(propan-2-yl)pyridin-4(1H)-one (3.60 g, 23.8 mmol) and phosphorous oxybromide (15.0 g, 52.3 mmol) in chloroform (10 mL) was heated at 130 °C in a sealed tube for 45 min. The reaction mixture was then cooled, quenched by the addition of ice, diluted with water (50 mL) and neutralized with solid sodium carbonate. The mixture was extracted with methylene chloride (2 × 75 mL) and the combined organic extracts were dried over Na₂SO₄. Evaporation of the solvents and purification by flash chromatography (silica gel, 80:20–50:50 ethyl acetate/hexanes) afforded 4-bromo-2-methyl-6-(propan-2-yl)pyridine as an orange oil (1.17 g, 23% yield): ¹H NMR (500 MHz, CDCl₃) δ 1.27 (d, *J* = 6.9 Hz, 6H, CHMe₂), 2.50 (s, 3H, Me), 2.99 (septet, *J* = 6.9 Hz, 1H, CHMe₂), 7.14 (s, 2H, Ar-H); MS *m/z* 214 (M+H)⁺.

5.3.5. Method E

5.3.5.1. Steps k–m. Preparation of 2,6-diethyl-4H-pyran-4-one (25). The reaction of 1,3-acetonedicarboxylic acid (15.0 g, 103 mmol) with propionic anhydride (41 mL, 320 mmol) in the presence of concentrated sulfuric acid (0.5 mL, 9 mmol) as described in the literature²² afforded 2,6-diethyl-4H-pyran-4-one as a pale yellow oil (6.03 g, 38% yield): ¹H NMR (300 MHz, CDCl₃) δ 1.23 (t, *J* = 7.5 Hz, 6H, 2 × CH₂CH₃), 2.54 (q, *J* = 7.5 Hz, 2 × CH₂CH₃), 6.08 (s, 2H, 2 × olefinic-H); MS *m/z* 153 (M+H)⁺.

5.3.5.2. Step n. 2,6-Diethylpyridin-4-ol (26). The reaction of 2,6-diethyl-4H-pyran-4-one (3.61 g, 23.7 mmol) and concentrated NH₄OH (15 mL, approx. 210 mmol) following the literature procedure gave 2,6-diethylpyridin-4-ol²³ as a viscous red oil (4.0 g, quantitative): ¹H NMR (300 MHz, CDCl₃) δ 1.25 (t, *J* = 7.6 Hz, 6H, 2 × CH₂CH₃), 2.67 (q, *J* = 7.6 Hz, 4H, 2 × CH₂CH₃), 6.22 (s, 2H, Ar-H); MS *m/z* 152 (M+H)⁺.

5.3.5.3. Step j. Preparation of 4-bromo-2,6-diethylpyridine (27). A mixture of 2,6-diethylpyridin-4-ol (3.58 g, 23.7 mmol) and phosphorous oxybromide (17.1 g, 59.6 mmol) was heated to 130 °C for 90 min, cooled to room temperature and the flask then placed in an ice bath. Ice was added in small pieces, and vigorous gas evolution was observed. The mixture was diluted with water (100 mL) and carefully neutralized by adding solid sodium carbonate in small portions. Once neutral, the aqueous layer was extracted with methylene chloride (2 × 100 mL), and the combined organic extracts were dried over Na₂SO₄. Evaporation of the solvents and purification by flash chromatography (silica gel, 1:9 ethyl acetate/hexanes) afforded 4-bromo-2,6-diethylpyridine as

an orange oil (3.86 g, 76% yield): ¹H NMR (300 MHz, CDCl₃) δ 1.28 (t, *J* = 7.6 Hz, 6H, 2 × CH₂CH₃), 2.77 (q, *J* = 7.6 Hz, 4H, 2 × CH₂CH₃), 7.16 (s, 2H, Ar-H); MS *m/z* 214 (M+H)⁺.

5.4. Separation of enantiomers (5S)-2-amino-5-(2,6-diethylpyridin-4-yl)-3-methyl-5-[3-(pyrimidin-5-yl)phenyl]-3,5-dihydro-4H-imidazol-4-one and (5R)-2-amino-5-(2,6-diethylpyridin-4-yl)-3-methyl-5-[3-(pyrimidin-5-yl)phenyl]-3,5-dihydro-4H-imidazol-4-one

Racemic mixture of 2-amino-5-(2,6-diethylpyridin-4-yl)-3-methyl-5-[3-(pyrimidin-5-yl)phenyl]-3,5-dihydro-4H-imidazol-4-one was separated to its two enantiomers by HPLC on Chiralcel AD, 2 × 25 cm using mobile phase 15% EtOH in hexane and a flow rate of 20 mL/min to afford (5S)-2-amino-5-(2,6-diethylpyridin-4-yl)-3-methyl-5-[3-(pyrimidin-5-yl)phenyl]-3,5-dihydro-4H-imidazol-4-one: [α]_D²⁵ = -0.035 (*c* = 1% in CH₃OH); ¹H NMR (DMSO-*d*₆ 300 MHz) δ 1.15 (t, *J* = 7.56 Hz, 6H, 2 × CH₂CH₃), 2.63 (q, *J* = 7.56 Hz, 4H, 2 × CH₂CH₃), 2.95 (s, 3H, Me), 6.72 (br s, 2H, NH₂), 7.15 (s, 2H, Ar-H), 7.45 (t, *J* = 7.69 Hz, 1H, Ar-H), 7.51 (d, *J* = 8.05 Hz, 1H, Ar-H), 7.62 (dd, *J* = 7.68, 1.46 Hz), 1H, Ar-H), 7.75 (t, *J* = 1.59 Hz, 1H, Ar-H), 8.95 (s, 2H, Ar-H), 9.15 (s, 1H, Ar-H); MS *m/z* (M+H)⁺ 401. Anal. Calcd for C₂₃H₂₄N₆O × 0.5 H₂O: C, 67.46; H, 6.15; N, 20.52. Found: C, 67.42; H, 5.96; N, 20.23; and (5R)-2-amino-5-(2,6-diethylpyridin-4-yl)-3-methyl-5-[3-(pyrimidin-5-yl)phenyl]-3,5-dihydro-4H-imidazol-4-one: [α]_D²⁵ = +0.039 (*c* = 1% in CH₃OH); ¹H NMR (DMSO-*d*₆ 300 MHz) δ 1.15 (t, *J* = 7.56 Hz, 6H, 2 × CH₂CH₃), 2.63 (q, *J* = 7.56 Hz, 4H, 2 × CH₂CH₃), 2.95 (s, 3H, Me), 6.72 (br s, 2H, NH₂), 7.15 (s, 2H, Ar-H), 7.45 (t, *J* = 7.69 Hz, 1H, Ar-H), 7.51 (d, *J* = 8.05 Hz, 1H, Ar-H), 7.62 (dd, *J* = 7.68, 1.46 Hz), 1H, Ar-H), 7.75 (t, *J* = 1.59 Hz, 1H, Ar-H), 8.95 (s, 2H, Ar-H), 9.15 (s, 1H, Ar-H); MS *m/z* (M+H)⁺ 401. Anal. Calcd for C₂₃H₂₄N₆O × 0.7 H₂O: C, 66.87; H, 6.19; N, 20.3. Found: C, 66.89; H, 5.81; N, 20.0.

5.5. Biological methods

5.5.1. FRET-based peptide cleavage assays

A homogenous, continuous fluorescence resonance energy transfer (FRET) was used to assess compound inhibition for BACE1, BACE2, cathepsin D, pepsin and renin activities.²⁴ The BACE1 and BACE2 activities were based on the cleavage of peptide substrate Abz-SEV-NLDAEFR-Dpa (Swedish substrate), while peptide substrate MOCAC-GKPIFFRLK (Dnp)-D-R-NH₂ was used for cathepsin D and Pepsin, and peptide substrate RE(EDANS)-IHPFHLVIHTK(DABCYL)-R for Renin. Kinetic rates were calculated and IC₅₀ values were determined by fitting the % inhibition, as a function of compound concentration, to the Hill equation ($y = ((B * Kn) + (100 * xn)) / (Kn + xn)$). (*x* is the agonist concentration and *y* is response (binding). *B*_{max} is the maximal or asymptotic response as *x* increases without bound. *K* is the EC₅₀. The Hill equation has no obvious physical interpretation. The role of the parameter *n* is to adjust the steepness of the curve).

5.5.2. Cell-based Aβ inhibition assay

CHO-K1 cells recombinantly expressing human wild-type APP (CHO-WT) were grown to confluence and then treated with serum free medium (Ultrapulture) supplemented with test compound in DMSO or DMSO alone (vehicle) at a final [DMSO] of 0.1% (v/v). Conditioned medium was harvested at 24 h, and assayed using streptavidin MSD plates, and an electrochemiluminescent immunoassay with biotinylated mouse monoclonal antibody 6E10 (Signet, Dedham, MA) as capture, and rabbit anti-Aβ₄₀ or Aβ₄₂ antibodies (Biosource, Camarillo, CA) as detection antibodies, with a secondary of MSD ECL tagged Sheep anti Rabbit for electrochemiluminescent amplification.

Data analysis of the MSD assay was performed by fitting the percent inhibition, as a function of compound concentration, to a

four-parameter logistic curve and the concentration at which the cellular production of A β 40 or A β 42 was reduced by 50% (EC₅₀) was determined. Compound toxicity was assessed via mitochondrial function using an MTS readout (MTS kit from Promega); values are represented as LD₅₀ or the dose of compound that resulted in 50% of control signal (e.g., 50% of the highest MTS signal).

5.6. X-ray crystallography

5.6.1. Cloning/expression of BACE1

A human BACE1 secreting mammalian secreting cell line (CHO cell line) was made by expressing a construct in which the prodomain plus ectodomain of human BACE1 (residues 22–454) was fused to the honeybee melittin secretory leader sequence at the 5' end and the Fc region of IgG, separated from the BACE sequence via an enterokinase cleavage site, was fused at the 3' end of BACE1. The BACE1/Fc fusion protein was affinity purified by protein-A sepharose and removal of the Fc domain was achieved with enterokinase cleavage. Purified BACE1 protein was accomplished via sequential size-exclusion chromatography. *Escherichia coli*-derived expression material was used for co-crystallographic studies. A codon-derived BACE1 *E. coli* expression construct was fused to a carboxy-terminal 6X HIS tag. After scale up, inclusion bodies were purified and protein refolded and dialyzed. The pro domain was cleaved with furin and BACE1 was further purified by size exclusion chromatography. The refolded *E. coli*-derived BACE1 showed the same enzymatic activity as the CHO-derived material (data not shown).

5.6.2. Crystallization and X-ray diffraction analysis of BACE1

Crystals were grown by hanging drop vapor diffusion at 18 °C in drops containing 1.0 μ L protein stock solution (200 μ M protein, 20 mM Tris–HCl, pH 7.5, 250 mM NaCl, and 240 μ M compound of interested diluted from a 100 mM stock in DMSO) mixed with 1.0 μ L well solution (6% PEG 3350, 0.1 M sodium acetate pH 5.4) end equilibrated against 0.5 mL well solution. Rod shaped crystals grew in several days.

5.6.3. Data collection

Crystals were drawn through a solution of 25% glycerol and 75% well solution, and cooled rapidly in liquid nitrogen. Diffraction data were recorded at the ALS beamline 5.0.1 on a q-210 ccd camera. Intensities were integrated and scaled using the programs DENZO and SCALEPACK.²⁵

5.6.4. Phasing, model building and refinement

Structures were determined by molecular replacement using AmorE²⁶ and the apo structure of BACE1 (PDB ID 1W50) as the search model. The final structures were obtained after several iterative cycles of refinement using Phenix²⁷ and model improvement in Coot.²⁸

5.6.5. Data deposition

The atomic coordinates of the BACE1 crystal structure for compounds **3b** (3INF)¹⁵, **30** (3IN3), **38** (3IN4) have been deposited in the Protein Data Bank, Research Collaboratory for Structural Bioinformatics, Rutgers University, New Brunswick, New Jersey. The atomic coordinates of the apo-BACE2 structure (2EWY) were obtained from the Protein Data Bank.

5.7. Molecular modeling. Docking calculations were performed using the QXP software package²⁹

Once the X-ray ligands were minimized in the active site, constrained simulated annealing calculations were performed to relieve any artifacts of the X-ray refinement perceived as unfavorable interactions or strain by the modified AMBER force field with QXP. The X-ray ligand was then redocked to confirm that the lowest energy pose is in agreement with the X-ray structure. Once the binding site model was generated, docking of analogues was performed using the QXP Monte Carlo docking algorithm mcdock in combination with combidock. Visualization of X-ray structures and docking results was performed using the InsightII software package (www.accelrys.com, Accelrys, Inc., San Diego, CA). Conformational analysis was performed using MacroModel (MacroModel 8.0; Schrodinger, LLC, Portland, OR), with the OPLS-AA force fields, and a GBSA solvation model.

Supplementary data

X-ray crystallographic data (collection details, refinement statistics), ¹HNMR and analytical data of the final compounds not listed in the Experimental Section, and supplemental information of biological assays are available. Supplementary data associated with this article can be found, in the online version, at doi:10.1016/j.bmc.2009.12.007.

References and notes

- Dickson, D. W. *J. Neuropathol. Exp. Neurol.* **1997**, *56*, 321–339.
- Selkoe, D. J. *Science* **1997**, *275*, 630–631.
- Vassar, R.; Citron, M. *Neuron* **2000**, *27*, 416–422.
- Selkoe, D. J. *Physiol. Rev.* **2001**, *81*, 741–766.
- Selkoe, D. J. *Ann. Intern. Med.* **2004**, *140*, 627–638.
- Arendt, T. *Neuroscience* **2001**, *102*, 723–765.
- Hardy, J.; Selkoe, D. J. *Science* **2002**, *297*, 353–356.
- Selkoe, D. *Ann. N.Y. Acad. Sci.* **2000**, *924*, 17–25.
- Couglan, C.; Breen, K. C. *Pharm. Ther.* **2000**, *86*, 111–144.
- Racchi, M.; Govone, S. *Trends Pharmacol. Sci.* **1999**, *20*, 418–423.
- Checler, F. J. *Neurochem.* **1995**, *65*, 1431–1444.
- Malamas, M. S.; Erdei, J.; Gunawan, I.; Barnes, K.; Johnson, M.; Hui, Y.; Turner, J.; Hu, Y.; Erik Wagner, E.; Fan, K.; Olland, A.; Bard, J.; Robichaud, A. *J. Med. Chem.* **2009**, *52*, 6314–6323.
- Malamas, M. S.; Barnes, K.; Johnson, M.; Hui, Y.; Zhou, P.; Turner, J.; Hu, Y.; Erik Wagner, E.; Fan, K.; Olland, A.; Bard, J.; Jacobsen, S.; Ronald L. Magolda, R.; Pangalos, M.; Robichaud, A. *J. Med. Chem.*, (online 7 December 2009).
- Dominguez, D.; Tournoy, J.; Hartmann, D.; Huth, T.; Cryns, K.; Deforce, S.; Serneels, L.; Camacho, I. E.; Marjaux, E.; Craessaerts, K.; Roebroek, A. J. M.; Schwake, M.; D'Hooge, R.; Bach, P.; Kalinke, U.; Moechars, D.; Alzheimer, C.; Reiss, K.; Paul Saftig, P.; De Strooper, B. *J. Biol. Chem.* **2005**, *280*, 30797–30806.
- Kagedal, K.; Johansson, U.; Llinger, K. O. *FASEB* **2001**, *15*, 1592–1594.
- Sonogashira, K.; Tohda, Y.; Hagihara, N. *Tetrahedron Lett.* **1975**, *50*, 4467–4470.
- Miyaura, N.; Suzuki, A. *Chem. Rev.* **1995**, *95*, 2457–2483.
- Comins, D. L.; Mantlo, N. B. *J. Org. Chem.* **1985**, *50*, 4410–4411.
- Ciana, L. D.; Haim, A. *J. Heterocycl. Chem.* **1984**, *21*, 607–608.
- Dixon, J. WO 035507, 2005.
- Beak, P.; Covington, J.; Smith, S.; White, M.; Zeigler, J. *J. Org. Chem.* **1980**, *45*, 1354–1362.
- Yates, P.; Hand, E. S.; Singh, P.; Roy, S. K.; Still, W. J. *J. Org. Chem.* **1969**, *34*, 4046.
- Deshapande, S. *J. Indian Chem. Soc.* **1932**, *303*.
- Wu, P.; Brand, L. *Anal. Biochem.* **1994**, *218*, 1–13.
- Otwinowski, Z.; Minor, W. *Methods Enzymol.* **1997**, *276*, 307–326. MacroMol. Crystallogr., Part A.
- CCP4 *Acta Crystallogr., Sect. D Biol. Crystallogr.* **1994**, *50*, 760–763.
- Adams, P. D.; Grosse-Kunstleve, R. W.; Hung, L.-W.; Ioerger, T. R.; McCoy, A. J.; Moriarty, N. W.; Read, R. J.; Sacchettini, J. C.; Sauter, N. K.; Terwillinger, T. C. *Acta Crystallogr., Sect. D* **2002**, *58*, 1948–1954.
- Emsley, P.; Cowtan, K. *Acta Crystallogr., Sect. D Biol. Crystallogr.* **2004**, *60*, 2126–2132.
- McMartin, C.; Bohacek, R. S. *J. Comput. Aided Mol. Des.* **1997**, *11*, 333–344.